

Quantum jump photodetector for narrowband photon counting with a single atom

Laura Zarraoa,^{1,*} Romain Veyron,¹ Tomas Lamich,¹ and Morgan W. Mitchell^{1,2,†}

¹*ICFO - Institut de Ciències Fotoniques, The Barcelona Institute of Science and Technology, 08860 Castelldefels, Barcelona, Spain*

²*ICREA - Institució Catalana de Recerca i Estudis Avançats, 08010 Barcelona, Spain*

Using a single neutral ^{87}Rb atom held in an optical trap, and “quantum jump” detection of single-photon-initiated state changes, we demonstrate an intrinsically-narrowband single-photon detector, of interest for separating weak signals from strong optical background. Using novel statistical analysis, we measure quantum efficiency of $2.9(2) \times 10^{-3}$, a record for single-pass quantum jump production, and dark counts of $9(20) \times 10^{-3}$ counts/s during passive accumulation plus $1.8(1) \times 10^{-2}$ counts per readout, orders of magnitude below those of traditional single-photon detectors. The 6 MHz detection bandwidth is orders of magnitude narrower than existing atomic filters. Available methods can substantially improve QJPD quantum efficiency, dark counts, bandwidth, and tunability.

Single-photon detection is a high-sensitivity technique used in many low-light sensing applications, for example laser ranging (LIDAR) [1], astronomical observation [2], and fluorescence microscopy [3]. Single-photon detection also enables efficient measurement of photon correlations, central to quantum optics [4, 5] and optical quantum technologies [6]. Most single-photon detectors function by transducing photon-induced processes in solid-state materials, e.g., photoionization from metals [7], electron-hole pair production in semiconductors [8–10] or heating of superconductors [11, 12]. In solid-state detectors, careful design and fabrication allows high quantum efficiency (QE) [13, 14], i.e., probability of faithfully detecting the presence of a photon. The use of low-defect materials and cryogenic temperatures can greatly reduce dark counts (DC) [15], i.e., detection events not caused by arriving photons.

A growing number of single-photon counting applications require, in addition to sensitivity, a strong rejection of background photons. Existing applications include free-space quantum communications [16], and “light-shining-through-walls” searches for dark matter [17, 18]. Emerging applications include near-space and deep-space classical communications [19] and spectroscopy of exoplanet atmospheres [20]. Solid-state detectors, because they are intrinsically broadband, must be complemented by filters if they are to be used in such background-sensitive applications. Narrowband filters reduce QE, and can be a source of background that increases DC.

In this context, it is interesting to consider photon counting methods based on the photoresponse of intrinsically-narrowband systems such as atoms. Available atomic systems have optical bandwidths ranging from a few GHz in hot vapor filters [21, 22] used for background rejection in LIDAR sky observation [23], to mHz in cold atoms on forbidden transitions [24]. Atomic resonance frequencies are fixed, but a detector based on atomic resonances can in principle detect any frequency through optical frequency conversion, which preserves

both photon number and quantum correlations [25]. A single atom typically has a low probability of interacting with a single passing photon, but this probability can be raised, in principle to unity, by high numerical aperture (high-NA) focusing [26, 27] or optical resonators [28].

Here we study the use of a single cold, trapped neutral atom with 6 MHz optical bandwidth as a single-photon detector based on “quantum jump” (QJ) techniques, i.e., we demonstrate a quantum jump photodetector (QJPD). We describe the nature of QE and DC in this system, which resembles CCD [8] and CMOS [9, 10] detectors in that it has separated acquisition and readout time windows with distinct dark count contributions. We introduce methodology, specific to the QJPD scenario, for establishing the QE and DC contributions in quantum jump photodetection. Using a single ^{87}Rb atom as a photodetector for 780 nm light, we demonstrate a QE of $2.9(2) \times 10^{-3}$ (a record for a single atom in free space), a dark current of $9(20) \times 10^{-3}$ counts/s, i.e., consistent with zero and limited by measurement statistics, and a readout contribution of $1.8(1) \times 10^{-2}$ counts per readout. The DC of the QJPD are already competitive with any non-cryogenic detector, and could benefit from several proven atomic and optical techniques. As noted already, the QE can in principle be raised close to unity through various enhancement techniques.

QJs, first studied experimentally in single trapped ions [29], are abrupt transitions of an atom between states or groups of states with observably different fluorescence behavior. We illustrate this with the ^{87}Rb D₂ transitions, from 5S_{1/2} F (ground states) to 5P_{3/2} F' (excited states), as shown in Fig. 1b. When illuminated with laser light tuned to the closed $F = 2 \rightarrow F' = 3$ “cooler” transition, the $F = 2$ ground state continuously emits resonance fluorescence. Under the same illumination, the $F = 1$ ground state produces negligible fluorescence, because of the larger detuning from any allowed transition. Absorption of a single “probe” photon tuned to the $F = 1 \rightarrow F' = 2$ transition, followed by sponta-

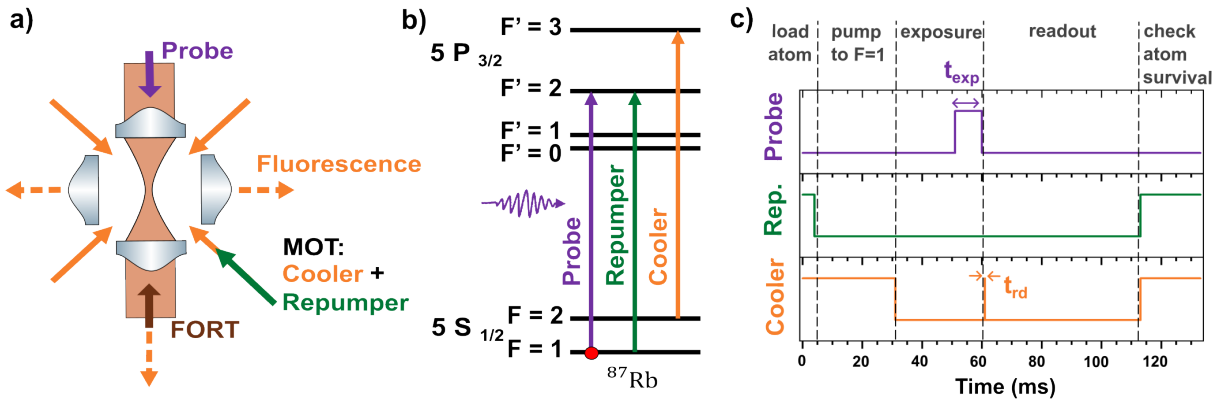


FIG. 1. Overview of the QJPD operation. a) Experimental set-up consisting of four high numerical aperture lenses in a Maltese cross configuration. b) Lambda system in which the ^{87}Rb QJPD operates. c) Experimental sequence used for quantum jump detection: an atom is loaded into the trap, prepared in the $F = 1$ ground state, exposed to probe photons during an exposure time t_{exp} , and has its state “read out” by exposure to cooler light for time t_{rd} . MOT light including repumper is then applied to check if the atom is still in the trap.

neous emission to the $F = 2$ ground state, thus induces a transition between a low- and high-fluorescence condition, which can be detected by collecting and counting the resonance fluorescence photons. In effect, the probe photon, by causing a change of atomic state, triggers a cascade of resonance fluorescence events.

A practical sequence is shown in Fig. 1c: the atom is initialized in state $F = 1$, exposed to probe light during an exposure time window and then read out by illumination with cooler light. During exposure, an incoming probe photon promotes the atom to $F' = 2$ with probability η_{abs} , determined by the matching of the incoming photon properties (spatial, spectral, and polarization) to the allowed $F = 1 \rightarrow F' = 2$ transitions [26, 30]. From the $F' = 2$ state, the atom falls to the $F = 1$ ($F = 2$) state with probability q ($1 - q$), in our example $1/2$ ($1/2$), determined by the branching ratio.

If the atom falls to the initial state, in our example $F = 1$, the absorption event has failed to produce a quantum jump. The efficiency for producing a jump is thus $\eta_{\text{QJ}} = q\eta_{\text{abs}}$, in our example $\eta_{\text{QJ}} = \eta_{\text{abs}}/2$. Meanwhile, for a natural-lifetime limited transition and a single-pass interaction of the probe photon with the atom, η_{QJ} is upper-bounded by q , so that $\eta_{\text{QJ}} \leq q(1 - q)$, which saturates at $1/4$ for a 1:1 branching ratio, as is the case for our system.

During the readout, an atom in $F = 2$ experiences a stochastic evolution, in which the atom can repeatedly scatter photons via the $F' = 3$ or $F' = 2$ state to return to $F = 2$, and with a smaller probability scatter a photon via $F' = 2$ or $F' = 1$ to fall to $F = 1$, at which point the fluorescence ceases. The scattered photons are collected and detected by single-photon avalanche diodes (SPADs). The net efficiency, i.e., probability that a scattered photon is collected and produces a SPAD event, is η_{det} , and

we write the probability distribution for the number of detected fluorescence photons as $f_{\eta_{\text{det}}}(n_{\text{fl}}|F = 2)$. The observed count is $n_c = n_{\text{fl}} + n_{\text{bg}}$, where n_{bg} is the detector background counts, assumed Poissonian. n_c has distribution

$$P(n_c|F = 1) = \mathcal{P}_{\mu_{\text{bg}}}(n_c) \quad (1)$$

$$P(n_c|F = 2) = [\mathcal{P}_{\mu_{\text{bg}}}(n_{\text{bg}}) * P_{\eta_{\text{det}}}(n_{\text{fl}}|F = 2)](n_c), \quad (2)$$

where $\mathcal{P}_{\mu}(n) \equiv \exp[-\mu]\mu^n/n!$ is the Poisson distribution with mean μ , and $*$ indicates convolution. A specific model for $P_{\eta_{\text{det}}}(n_{\text{fl}}|F = 2)$, appropriate for homogeneously broadened systems, is given in the Appendix.

We implement a QJPD using a single neutral ^{87}Rb atom in a strongly-focused far-off-resonance trap (FORT) surrounded by high-NA lenses. The experimental system is shown schematically in Fig. 1a, and is described in detail in [31, 32]. In the following, all laser detunings are given with respect the natural ^{87}Rb transitions. The atom experiences dynamical Stark shifts induced by the FORT [33, 34]: at trap center, the light shift of the $F = 1 \rightarrow F' = 2$ transition is $3.3\Gamma_0$ and scalar, with negligible tensor contribution. For the cooler transition, the tensorial polarisability leads to Zeeman-state-dependent excited state light shifts, ranging from $2.6\Gamma_0$ ($m_{F'} = \pm 3$) to $4.2\Gamma_0$ ($m_{F'} = 0$). Lenses surround the atom in the horizontal plane. The FORT and probe polarizations, as well as an applied bias magnetic field of 180 mG , are vertical, which we take as the quantization axis.

The atom is loaded from a three-dimensional magneto-optical trap (MOT) into the FORT, with depth $787(2)\text{ }\mu\text{K}$. The atom is cooled by polarization gradient cooling for 4 ms at a detuning of $3.75\Gamma_0$ to the red of the $F = 2 \rightarrow F' = 3$ transition and intensity of 42 W/m^2 per MOT beam.

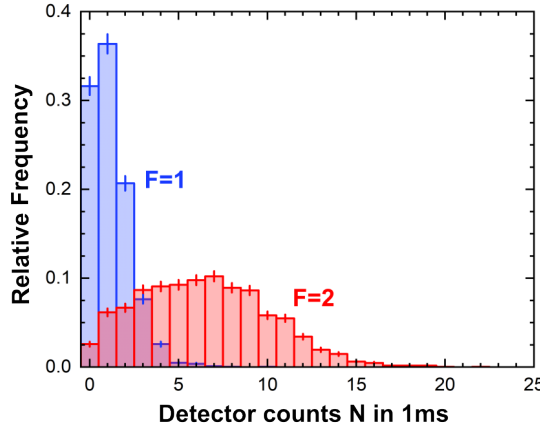


FIG. 2. Experimental characterization of the state-dependent fluorescence of the atom: histograms show $f(n_c|F)$, the number of counts n_c collected when an atom, initially prepared in the $F = 1$ (blue) or $F = 2$ (red) ground state, is illuminated for 1 ms by cooler light. n_c is obtained by summing SPAD detection events from light collected by two high-NA lenses, one along the trap axis and one transverse to the axis.

We first measure the conditional count distributions of Eqs. (1) and (2), by optically pumping the atom to $F = 1$ or $F = 2$, respectively, and reading out their fluorescence. As illustrated in Fig. 1c, the atom is prepared in the $F = 1$ ground state by a 27 ms duration pulse tuned $3\Gamma_0$ to the red of the $F = 2 \rightarrow F' = 3$ transition. The $F = 2$ preparation (not shown in Fig. 1c) is performed by illuminating with a 10 ms pulse tuned $5\Gamma_0$ to the blue of the $F = 2 \rightarrow F' = 3$ transition.

The trap depth is then lowered to 558(2) μK to reduce the FORT-induced differential light shifts on the $F' = 3$ state. At this stage the atom temperature is 15(2) μK . The atom is then illuminated by a readout pulse of all MOT beams with duration $t_{\text{rd}} = 1$ ms, intensity 20 W/m^2 per beam, and tuned $0.5\Gamma_0$ to the blue of the $F = 2 \rightarrow F' = 3$ transition. Fluorescence photons during this time are collected through three NA = 0.5 aspheric lenses and counted by SPADs (Excelitas SPCM-AQ4C). Their histograms, relative frequencies $f(n_c|F = 1)$ and $f(n_c|F = 2)$, are shown in Fig. 2, and are well approximated by a Poisson distribution with $\mu = 1.146(2)$, and by a Gaussian with mean 5.9(1) and variance 17.6(8), respectively.

From Eqs. (1) and (2), $P(n_c|F)$ is nonvanishing for any n_c and F , meaning we cannot unambiguously infer F from n_c and must resort to decision theory [35]. Because the QJ increases the fluorescence rate of the atom, it is natural to define detection (D) of the QJ as $n_c > n_{\text{thr}}$ and non-detection (ND) as $n_c \leq n_{\text{thr}}$, where n_{thr} is a threshold to be chosen in function of the cost of false negatives $\epsilon_{\text{FN}} \equiv P(n_c \leq n_{\text{thr}}|F = 2)$, which decrease QE, and false positives $\epsilon_{\text{FP}} \equiv P(n_c > n_{\text{thr}}|F = 1)$, which

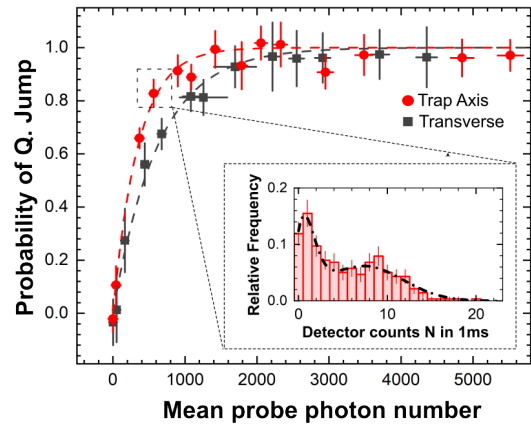


FIG. 3. Probabilities $P(\text{QJ}|\bar{n}_{\text{pr}})$ of a quantum jump versus mean number of probe photons \bar{n}_{pr} illuminating the atom. Symbols show $P(\text{QJ}|\bar{n}_{\text{pr}})$, calculated using Eq. (3). Y axis error bars show $\pm 1\sigma$ uncertainty computed using Eq. (4). X axis error bars show combined statistical (from fluctuation during acquisition) and systematic (from probe power calibration) uncertainty in \bar{n}_{pr} . Dashed lines show fits with Eq. (6) with results: $\eta_{\text{QJ}} = 2.9(2) \times 10^{-3}$ for illumination along the trap axis (red), and $\eta_{\text{QJ}} = 1.60(6) \times 10^{-3}$ for illumination orthogonal to the trap axis (black). Inset shows a histogram of n_c (red bars) for probe illumination with $\bar{n}_{\text{pr}} = 570(40)$ photons and the fit (black dashed line) with Eq. (5) to obtain $P(\text{QJ})$.

contribute to readout noise. Although other choices may better suit specific applications, here we choose $n_{\text{thr}} = 4$, which maximizes readout fidelity $\mathcal{F} \equiv 1 - (\epsilon_{\text{FP}} + \epsilon_{\text{FN}})/2$ as defined by Fuhrmanek et al. [36], to give $\mathcal{F} = 0.72$.

Given n_{thr} and $P(n_c|F)$, and thus $P(\text{D}|F)$, the probability of a quantum jump $P(\text{QJ})$ can be estimated as:

$$P(\text{QJ}) = \frac{P(\text{D}) - \epsilon_{\text{FP}}}{1 - \epsilon_{\text{FP}} - \epsilon_{\text{FN}}}. \quad (3)$$

The uncertainty in this inference can be calculated by error propagation: For the binomial outcome D/ND, the mean-squared error of $P(\text{QJ})$ is:

$$\text{MSE}[P(\text{QJ})] = \frac{1}{(1 - \epsilon_{\text{FP}} - \epsilon_{\text{FN}})^2} \frac{P(\text{D})[1 - P(\text{D})]}{N_{\text{runs}}}, \quad (4)$$

where N_{runs} is the number of repetitions of the experiment. Eqs. (3) and (4) will be used to estimate the number of QJs and its uncertainty when characterizing quantum efficiency and dark counts, e.g., for Fig. 3.

Because the QJPD detects photons in two steps, namely the $F = 1 \rightarrow F = 2$ state change that is the QJ itself and the subsequent observation by resonance fluorescence, we can identify two QEs: the QJ efficiency η_{QJ} and the detection efficiency η_{det} . To measure these, we use the sequence shown in Fig. 2c with pulse durations and power levels as given above, with the addition of a strongly-attenuated laser probe pulse of duration

$t_{\text{exp}} = 10$ ms, detuned $3\Gamma_0$ from the $F = 1 \rightarrow F' = 2$ transition, focused onto the atom by one of the high-NA lenses and of variable mean photon number \bar{n}_{pr} . To monitor the probe photon number, the probe light is split by a 50:50 fiber beamsplitter, with one output going directly to one SPAD, and the other to the QJPD. The SPAD reading is calibrated against power-meter measurements before and after the vacuum chamber housing the atom, assuming equal attenuation by the windows.

For each probe power setting, 300 runs of the prepare-probe-readout sequence are made to build a histogram of n_c , as illustrated in 3, inset. This is fitted with

$$P(n_c|\bar{n}_{\text{pr}}) = P(n_c|F=1)P(F=1|\bar{n}_{\text{pr}}) + P(n_c|F=2)P(F=2|\bar{n}_{\text{pr}}), \quad (5)$$

which describes a weighted sum of the conditional probabilities of Eqs. (1) and (2) with a single fit parameter $P(\text{QJ}|\bar{n}_{\text{pr}}) \equiv P(F=2|\bar{n}_{\text{pr}}) = 1 - P(F=1|\bar{n}_{\text{pr}})$. The resulting values of $\eta_{\text{QJ}}(\bar{n}_{\text{pr}})$, both for illumination along the trap axis and transverse to the trap axis, are shown in 3, and are well described by single-parameter saturation curves

$$P(\text{QJ}|\bar{n}_{\text{pr}}) = 1 - \exp[-\eta_{\text{QJ}}\bar{n}_{\text{pr}}], \quad (6)$$

with quantum jump efficiency $\eta_{\text{QJ}} = 2.9(2) \times 10^{-3}$ for illumination along the trap axis, and $\eta_{\text{QJ}} = 1.60(6) \times 10^{-3}$ for illumination orthogonal to the trap axis. The higher coupling efficiency along the trap axis is expected, as the atom spends more time in the light's path due to the elongated shape of the atomic probability distribution along the FORT axis. These η_{QJ} values are the highest quantum jump probabilities yet reported for free-space single-photon level coupling to either neutral atoms or to ions [37].

To understand dark counts in the QJPD, we study the two distinct sources of detections in the absence of incoming probe photons. First, there is a finite probability for a quantum jump during the exposure phase, e.g., due to scattering of FORT light. Second, there are false positives in the readout process. These two sources play the same roles, respectively, as “dark current” and “readout noise” in a CCD [8] or CMOS sensor [10], and we will use those names here. They imply a dark count rate that depends on the readout frequency, and thus on the time resolution of the acquisition.

To quantify the readout noise, we prepare the atom in $F = 1$, wait 37 ms, equal to the exposure window when measuring QE, apply a readout pulse of duration t_{rd} , record the resulting n_c and infer D/ND by comparison to n_{thr} defined above. For each t_{rd} value, 500 runs are acquired. Runs in which the atom is not present after the sequence are discarded. The mean rate of detection r_{count} is computed as the net number of D events divided by the net illumination time. By linear regression

of r_{count} versus t_{rd} , we find out a readout error rate of 18(1) counts/s of readout duration. Our readout pulse is 1 ms in duration, for a false positive probability of $P(\text{D}|F=1) = 1.8(1) \times 10^{-2}$, or $1.8(1) \times 10^{-2}$ dark counts per read.

The dark current is quantified in a similar manner: The atom is prepared in $F = 1$, remains trapped, illuminated only by the trapping light for time t_{exp} , after which it is read out with a 1 ms pulse to find n_c and infer D/ND. We make 500 runs each for $t_{\text{exp}} = 0.5$ s, 1 s, 2 s and 3 s, limited by the trap lifetime due to background gas collisions, and discard runs with lost atoms. A linear regression of the number of D events versus accumulated exposure time finds a dark current rate of $9(20) \times 10^{-3}$ counts/s. This result, consistent with zero, is limited by the false positive rate and the number of atoms tested. It places an upper limit on the dark current contribution to the QJPD DC. At 1 Hz readout rate, the net dark counts are far below those of commercially-available single-photon detectors, including photomultipliers [7], semiconductor devices [8–10, 38], and superconducting devices [12, 39] but exceed those of some research superconducting detectors [11, 15, 17].

Several proven techniques could improve QJPD performance. Readout noise can be reduced by Zeeman-state pumping during readout [36], using SNSPD in place of SPADs, and improved vacuum to extend trap lifetime. These would increase the statistical distance between $P(n_c|F=1)$ and $P(n_c|F=2)$ and thus reduce false positives. Dark current, too small to measure in this experiment, can be produced by off-resonance optical excitation by FORT light or thermal photons, or by magnetic excitation of the ground-state hyperfine transition. We estimate the FORT to be the strongest contributor, with thermal and magnetic background being negligible. A blue-detuned FORT or lattice, which traps the atom at an intensity minimum, could thus reduce the dark current. A magic wavelength optical trap could in addition reduce optical linewidth broadening [40]. Non-optical trapping, e.g., for ions [41], similarly escapes these effects. QE can be increased by initializing the atom in a specific m_F state [41, 42], and by optical methods including strong beamshaping [27] and cavity enhancement [43]. Cavity-QED methods can moreover escape the $\eta_{\text{QJ}} \leq 1/4$ efficiency limit in driving Raman transitions such as $F = 1 \rightarrow F = 2$ [42].

In conclusion, we have demonstrated quantum jump photon detector (QJPD) with an intrinsically narrow 6 MHz response bandwidth. We introduce and demonstrate methodology for measuring the two quantum efficiencies and the two dark count contributions of a QJPD, and find dark counts below those of any commercially-available single-photon detector. The QJPD technique may be interesting for the growing number of applica-

tions in communications and fundamental science that require high sensitivity and strong background rejection through frequency discrimination. Several proven atomic and optical technologies could be applied to reach different wavelength ranges, narrower bandwidths, higher quantum efficiency, and lower dark counts.

Acknowledgements: We thank L. C. Bianchet for her useful insight on quantum jump techniques in single atoms during our discussions. We also thank N. Alves and V. Prakash for helpful discussions. Funded by the European Union (ERC, Field-SEER, 101097313 and QUANTIFY, 101135931), NextGenerationEU/PRTR, and by the Spanish Ministry of Science MCIN: project SAPONARIA (PID2021-123813NB-I00) and “Severo Ochoa” Center of Excellence CEX2019-000910-S, Departament de Recerca i Universitats de la Generalitat de Catalunya grant No. 2021 SGR 01453, Fundació Privada Cellex, Fundació Mir-Puig. LZ acknowledges the “Presidencia de la Agencia Estatal de Investigación” grant Ref. PRE2020-094392. TL acknowledges Marie Skłodowska-Curie grant agreement No 847517. Views and opinions expressed are those of the authors only and do not necessarily reflect those of the European Union or the European Research Council Executive Agency. Neither the European Union nor the granting authority can be held responsible for them.

Appendix – Minimal stochastic model for $P(n_c|F = 2)$: The atom starts in $F = 2$, with probability p to go to $F = 2$, and probability $1 - p$ to go to $F = 1$, when scattering a photon. The probability to scatter exactly s photons before arriving to the $F = 1$ state and going dark is exponential: $P(n_{\text{scat}} = s) = p^{s-1}(1 - p)$ for $s \geq 1$ and zero otherwise. If the efficiency from scattering to detection is η , the probability of detecting $n_{\text{det}} = d$ photons out of s scattered photons is binomial: $P(n_{\text{det}} = d|n_{\text{scat}} = s) = \eta^d(1 - \eta)^{(s-d)} \binom{s}{d}$. Summing these conditional distributions, weighted by the probability to scatter s photons, we have the unconditional probability of detecting d photons: $P(n_{\text{det}} = d) = \sum_{s=d}^{\infty} P(n_{\text{det}} = d|n_{\text{scat}} = s)P(n_{\text{scat}} = s) = p^{d-1}(1 - p)\eta^d / (1 - p + \eta p)^{d+1}$. We convolve this with the Poisson distribution for the background counts to find the distribution for $n_c \equiv n_{\text{det}} + n_{\text{bg}}$:

$$P(n_c|F = 2) = \sum_{d=0}^{n_c} P(n_{\text{det}} = d) \frac{e^{-\mu} \mu^{n_c-d}}{(n_c - d)!} \quad (7)$$

$$= \frac{\mu^{n_c}}{n_c! p} x e^x E_{-n_c}[x + \mu], \quad (8)$$

where $x \equiv \mu(1 - p)/\eta p$ and $E_n[z]$ is the exponential integral function. $P(n_c|F = 2)$ can also be expressed in terms of the incomplete Gamma function. The fact that Eq. (8) does not fit well the $f(n_c|F = 2)$ of Fig. 2 suggests that inhomogeneity, e.g., in the response of different Zeeman states or to different cooler polarizations, plays an

important role in determining $P(n_c|F = 2)$. For this reason, we use a heuristic (Gaussian) distribution in fitting $f(n_c|F = 2)$.

* laura.zarraoa@icfo.eu

† morgan.mitchell@icfo.eu

- [1] D. M. Winker, M. A. Vaughan, A. Omar, Y. Hu, K. A. Powell, Z. Liu, W. H. Hunt, and S. A. Young, Overview of the CALIPSO mission and CALIOP data processing algorithms, *Journal of Atmospheric and Oceanic Technology* **26**, 2310 (2009).
- [2] A. B. Walter, N. Fruitwala, S. Steiger, J. I. Bailey, N. Zobrist, N. Swimmer, I. Lipartito, J. P. Smith, S. R. Meeker, C. Bockstiegel, G. Coiffard, R. Dodkins, P. Szypryt, K. K. Davis, M. Daal, B. Bumble, G. Collura, O. Guyon, J. Lozi, S. Vievard, N. Jovanovic, F. Martinache, T. Currie, and B. A. Mazin, The MKID exoplanet camera for Subaru SCExAO, *Publications of the Astronomical Society of the Pacific* **132**, 125005 (2020).
- [3] K. König, Review: Clinical in vivo multiphoton FLIM tomography, *Methods and Applications in Fluorescence* **8**, 034002 (2020).
- [4] M. Giustina, M. A. M. Versteegh, S. Wengerowsky, J. Handsteiner, A. Hochrainer, K. Phelan, F. Steinlechner, J. Kofler, J.-A. Larsson, C. Abellán, W. Amaya, V. Pruneri, M. W. Mitchell, J. Beyer, T. Gerrits, A. E. Lita, L. K. Shalm, S. W. Nam, T. Scheidl, R. Ursin, B. Wittmann, and A. Zeilinger, Significant-loophole-free test of Bell’s theorem with entangled photons, *Physical Review Letters* **115**, 250401 (2015).
- [5] L. K. Shalm, E. Meyer-Scott, B. G. Christensen, P. Bierhorst, M. A. Wayne, M. J. Stevens, T. Gerrits, S. Glancy, D. R. Hamel, M. S. Allman, K. J. Coakley, S. D. Dyer, C. Hodge, A. E. Lita, V. B. Verma, C. Lambrocco, E. Tortorici, A. L. Miggdall, Y. Zhang, D. R. Kumor, W. H. Farr, F. Marsili, M. D. Shaw, J. A. Stern, C. Abellán, W. Amaya, V. Pruneri, T. Jennewein, M. W. Mitchell, P. G. Kwiat, J. C. Bienfang, R. P. Mirin, E. Knill, and S. W. Nam, Strong loophole-free test of local realism, *Physical Review Letters* **115**, 250402 (2015).
- [6] H.-S. Zhong, H. Wang, Y.-H. Deng, M.-C. Chen, L.-C. Peng, Y.-H. Luo, J. Qin, D. Wu, X. Ding, Y. Hu, P. Hu, X.-Y. Yang, W.-J. Zhang, H. Li, Y. Li, X. Jiang, L. Gan, G. Yang, L. You, Z. Wang, L. Li, N.-L. Liu, C.-Y. Lu, and J.-W. Pan, Quantum computational advantage using photons, *Science* **370**, 1460 (2020).
- [7] Becker-Hickl, Cooled fast PMT modules: PMC-150, Datasheet db-pmc150-v02 (2023).
- [8] Oxford Instruments: iKon slow-scan large CCD cameras: iKon-XL 231, Datasheet iKonXL231SS 0622 R1 (2024).
- [9] Teledyne Technologies: Long exposure optimized CMOS camera: Retiga E20, Retiga E-Series CMOS Camera Datasheet Rev A0-01-28-2023 (2023).
- [10] Hamamatsu, ORCA-Quest qCMOS camera: C15550-20UP, Technical note Cat. No. SCAS0154E05 NOV/2023 HPK (2023).
- [11] J. Dreyling-Eschweiler, N. Bastidon, B. Döbrich, D. Horns, F. Januschek, and A. Lindner, Characterization, 1064 nm photon signals and background events of a tungsten TES detector for the ALPS experiment, *Journal*

of Modern Optics (2015).

[12] Single Quantum Eos: SNSPD closed-cycle system, Datasheet SQ A4 brochure v6 (2024).

[13] K. Sperlich and H. Stolz, Quantum efficiency measurements of (EM)CCD cameras: high spectral resolution and temperature dependence, *Measurement Science and Technology* **25**, 015502 (2013).

[14] H. Shao, B. Cheng, Y. Xu, and G. Song, Ultrahigh-quantum-efficiency and high-bandwidth nanowire array UTC-PDs working at 1064 nm, *Optical and Quantum Electronics* **54**, 15 (2021).

[15] Y. Hochberg, I. Charaev, S.-W. Nam, V. Verma, M. Colangelo, and K. K. Berggren, Detecting sub-GeV dark matter with superconducting nanowires, *Phys. Rev. Lett.* **123**, 151802 (2019).

[16] C.-Z. Peng, T. Yang, X.-H. Bao, J. Zhang, X.-M. Jin, F.-Y. Feng, B. Yang, J. Yang, J. Yin, Q. Zhang, N. Li, B.-L. Tian, and J.-W. Pan, Experimental free-space distribution of entangled photon pairs over 13 km: Towards satellite-based global quantum communication, *Physical Review Letters* **94**, 150501 (2005).

[17] J. Chiles, I. Charaev, R. Lasenby, M. Baryakhtar, J. Huang, A. Roshko, G. Burton, M. Colangelo, K. Van Tilburg, A. Arvanitaki, S. W. Nam, and K. K. Berggren, New constraints on dark photon dark matter with superconducting nanowire detectors in an optical haloscope, *Phys. Rev. Lett.* **128**, 231802 (2022).

[18] A. D. Spector, Light-shining-through-walls experiments, in *The Search for Ultralight Bosonic Dark Matter*, edited by D. F. Jackson Kimball and K. van Bibber (Springer International Publishing, Cham, 2023) pp. 255–279.

[19] S.-P. Chen, Performance analysis of near-earth, lunar and interplanetary optical communication links, *Optical and Quantum Electronics* **54**, 562 (2022).

[20] Z. Rustamkulov, D. K. Sing, S. Mukherjee, E. M. May, J. Kirk, E. Schlawin, M. R. Line, C. Piaulet, A. L. Carter, N. E. Batalha, J. M. Goyal, M. López-Morales, J. D. Lothringer, R. J. MacDonald, S. E. Moran, K. B. Stevenson, H. R. Wakeford, N. Espinoza, J. L. Bean, N. M. Batalha, B. Benneke, Z. K. Berta-Thompson, I. J. M. Crossfield, P. Gao, L. Kreidberg, D. K. Powell, P. E. Cubillos, N. P. Gibson, J. Leconte, K. Molaverdikhani, N. K. Nikolov, V. Parmentier, P. Roy, J. Taylor, J. D. Turner, P. J. Wheatley, K. Aggarwal, E. Ahrer, M. K. Alam, L. Alderson, N. H. Allen, A. Banerjee, S. Barat, D. Barrado, J. K. Barstow, T. J. Bell, J. Blecic, J. Brande, S. Casewell, Q. Changeat, K. L. Chubb, N. Crouzet, T. Daylan, L. Decin, J. Désert, T. Mikal-Evans, A. D. Feinstein, L. Flagg, J. J. Fortney, J. Harrington, K. Heng, Y. Hong, R. Hu, N. Iro, T. Kataria, E. M. R. Kempton, J. Krick, M. Lendl, J. Lillo-Box, A. Louca, J. Lustig-Yaeger, L. Mancini, M. Mansfield, N. J. Mayne, Y. Miguel, G. Morello, K. Ohno, E. Palle, D. J. M. Petit dit de la Roche, B. V. Rackham, M. Radica, L. Ramos-Rosado, S. Redfield, L. K. Rogers, E. L. Shkolnik, J. Southworth, J. Teske, P. Tremblin, G. S. Tucker, O. Venot, W. C. Waalkes, L. Welbanks, X. Zhang, and S. Zieba, Early release science of the exoplanet WASP-39b with JWST NIRSpec PRISM, *Nature* **614**, 659 (2023).

[21] J. A. Zielińska, F. A. Beduini, N. Godbout, and M. W. Mitchell, Ultranarrow Faraday rotation filter at the Rb D₁ line, *Opt. Lett.* **37**, 524 (2012).

[22] J. A. Zielińska, F. A. Beduini, V. G. Lucivero, and M. W. Mitchell, Atomic filtering for hybrid continuous-variable/discrete-variable quantum optics, *Opt. Express* **22**, 25307 (2014).

[23] Y. Xia, X. Cheng, Z. Wang, L. Liu, Y. Yang, L. Du, J. Jiao, J. Wang, H. Zheng, Y. Li, F. Li, and G. Yang, Design of a data acquisition, correction and retrieval of Na Doppler lidar for diurnal measurement of temperature and wind in the mesosphere and lower thermosphere region, *Remote Sensing* **15**, 10.3390/rs15215140 (2023).

[24] W. Bowden, R. Hobson, I. R. Hill, A. Vianello, M. Schioppo, A. Silva, H. S. Margolis, P. E. G. Baird, and P. Gill, A pyramid MOT with integrated optical cavities as a cold atom platform for an optical lattice clock, *Scientific Reports* **9**, 11704 (2019).

[25] X. Wang, X. Jiao, B. Wang, Y. Liu, X.-P. Xie, M.-Y. Zheng, Q. Zhang, and J.-W. Pan, Quantum frequency conversion and single-photon detection with lithium niobate nanophotonic chips, *npj Quantum Information* **9**, 38 (2023).

[26] M. K. Tey, G. Maslennikov, T. C. H. Liew, S. A. Aljunid, F. Huber, B. Chng, Z. Chen, V. Scarani, and C. Kurtsiefer, Interfacing light and single atoms with a lens, *New Journal of Physics* **11**, 043011 (2009).

[27] M. Sondermann, M. Fischer, and G. Leuchs, Prospects of trapping atoms with an optical dipole trap in a deep parabolic mirror for light–matter–interaction experiments, *Advanced Quantum Technologies* **3**, 2000022 (2020).

[28] C. H. Nguyen, A. N. Utama, N. Lewty, K. Durak, G. Maslennikov, S. Straupe, M. Steiner, and C. Kurtsiefer, Single atoms coupled to a near-concentric cavity, *Phys. Rev. A* **96**, 031802 (2017).

[29] W. Nagourney, J. Sandberg, and H. Dehmelt, Shelved optical electron amplifier: Observation of quantum jumps, *Phys. Rev. Lett.* **56**, 2797 (1986).

[30] S. A. Aljunid, G. Maslennikov, Y. Wang, H. L. Dao, V. Scarani, and C. Kurtsiefer, Excitation of a single atom with exponentially rising light pulses, *Phys. Rev. Lett.* **111**, 103001 (2013).

[31] N. Bruno, L. C. Bianchet, V. Prakash, N. Li, N. Alves, and M. W. Mitchell, Maltese cross coupling to individual cold atoms in free space, *Opt. Express* **27**, 31042 (2019).

[32] L. Bianchet, N. Alves, L. Zarraoa, N. Bruno, and M. Mitchell, Manipulating and measuring single atoms in the Maltese cross geometry, *Open Research Europe* **1**, 10.12688/openreseurope.13972.1 (2021).

[33] S. Coop, S. Palacios, P. Gomez, Y. N. M. de Escobar, T. Vanderbruggen, and M. W. Mitchell, Floquet theory for atomic light-shift engineering with near-resonant polychromatic fields, *Opt. Express* **25**, 32550 (2017).

[34] L. C. Bianchet, N. Alves, L. Zarraoa, T. Lamich, V. Prakash, and M. W. Mitchell, Quantum jump spectroscopy of a single neutral atom for precise sub-wavelength intensity measurements, *Phys. Rev. Res.* **4**, L042026 (2022).

[35] M. Peterson, *An Introduction to Decision Theory* (Cambridge University Press, 2017).

[36] A. Fuhrmanek, R. Bourgain, Y. R. P. Sortais, and A. Browaeys, Free-space lossless state detection of a single trapped atom, *Phys. Rev. Lett.* **106**, 133003 (2011).

[37] J. Volz, M. Weber, D. Schlenk, W. Rosenfeld, J. Vrana, K. Saucke, C. Kurtsiefer, and H. Weinfurter, Observation of entanglement of a single photon with a trapped atom,

Phys. Rev. Lett. **96**, 030404 (2006).

[38] Hamamatsu, Photon counting modules C11202 series: C11202-050, Datasheet Cat. No. KACC1207E07 Sep. 2022 DN (2022).

[39] M. Shaw, Superconducting nanowire single photon detectors for deep space optical communication, 683rd WE-Heraeus-Seminar (2018).

[40] S. Zhang, B. Tiwari, S. Ganesh, P. Ramchurn, K. Bongs, and Y. Singh, Blue-detuned optical lattice for Sr long-range interactions in 2022 Joint Conference of the European Frequency and Time Forum and IEEE International Frequency Control Symposium (EFTF/IFCS) (2022) pp. 1–3.

[41] N. Piro, F. Rohde, C. Schuck, M. Almendros, J. Huwer, J. Ghosh, A. Haase, M. Hennrich, F. Dubin, and J. Eschner, Heralded single-photon absorption by a single atom, Nat Phys **7**, 17 (2011).

[42] H. P. Specht, C. Nolleke, A. Reiserer, M. Uphoff, E. Figueroa, S. Ritter, and G. Rempe, A single-atom quantum memory, Nature **473**, 190 (2011).

[43] A. Kuhn, M. Hennrich, and G. Rempe, Deterministic single-photon source for distributed quantum networking, Physical Review Letters **89**, 067901 (2002).